Electronic Supplementary Material (ESI) for Journal of Materials Chemistry C.
This journal is © The Royal Society of Chemistry 2023

Supporting Information

Flame Retardant benzimidazole-Linked covalent organic framework as organic solution sponge for acceleration of Li^+-Ion migration in solid-state electrolyte

Han Zhang,[a] Ya-Ru Kong,[a] Jin Zhang,*[a, b] Xing-Yu Ren,[a] Xiao-Ming Ren*[a,c]

[a] State Key Laboratory of Materials-Oriented Chemical Engineering and College of Chemistry and Molecular Engineering, Nanjing Tech University, Nanjing 211816, P. R. China

[b] State Key Laboratory of Chemical Engineering, School of Chemical Engineering, East China University of Science and Technology, Shanghai 200237, P. R. China

[c] State Key Laboratory of Coordination Chemistry, Nanjing University, Nanjing 210023, P. R. China

* Correspondence authors

Email: 1084752558@qq.com (J.Z.)

xmren@njtech.edu.cn (X.M.R.)

Contents

Experimental Section

Methods of characterization

Powder X-ray diffraction (PXRD) data were collected on a Bruker D8 diffractometer with Cu Kα radiation (λ = 1.5418 Å), operated at 40 kV and 40 mA, in the 2θ range of 3–50° with 0.01°/step. Fourier-transform infrared (FT-IR) spectra were recorded on a Thermo Scientific Nicolet iS10 spectrophotometer. A Micromeritics ASAP 2020 analyzer was used for N_2 adsorption/desorption measurements. Solid state ^{7}Li cross polarization magic angle spinning nuclear magnetic resonance (^{7}Li CP-MAS NMR) spectra were recorded on a 600 MHz Bruker AVANCE III HD spectrometer. X-ray photoelectron spectroscopy (XPS) analyses were conducted on a Thermo Scientific K-Alpha instrument. Scanning electron microscopy (SEM) images were taken by using a Quanta FEG-450 field emission scan electron microscopy. High-resolution transmission electron microscopic (HRTEM) images were taken by using a FEI-Talos F200s transmission electron microscopy.

Ionic conductivity measurement

The ionic conductivity was evaluated by AC impedance measurement on a Gamry 600+ electrochemical workstation in an enclosed environment. The electrode is assembled inside an argon-filled glove box. The details are summarized as follow: the powder sample was added into a PEEK tube with a diameter of 10 mm, and two gold flakes (diameter of 10 mm) as electrodes were put into the tube from the ends, then, the sample is extruded into compressed particles in the tube through a specially made titanium alloy, the thickness of pellet is ~2 mm.

The Li-ion transference number (t_{Li+}) measurement

$$t_{\mathrm{Li+}} = \frac{I_S}{I_0}$$

Herein, I_S represent the steady current after polarization, and I_0 is initial current.

The lithium-ion transference number was evaluated by chronoamperometry on a

Gamry 600+ electrochemical workstation. Before the test, place the assembled symmetrical cell (Li|**$LiBF_4$/PC@PBI-COF/PTFE**|Li) in an oven at 80℃ to balance the potential and ensure that the initial state of the battery is consistent. The bias voltage of the symmetrical cells is set to 10 mV.

Electrochemical stability test

The electrochemical stability test was evaluated by linear sweep voltammetry (LSV) on a Gamry 600+ electrochemical workstation. Before the test, place the half-cell (Pt|**$LiBF_4$/PC@ PBI-COF/PTFE**|Li) in an oven at 80℃ to balance the potential. The half-cell was scanned from 2 to 7 V with a potential sweep speed of 5 mV s^{-1}, and the measurement was performed at room temperature.

Theoretic calculation in details

In order to facilitate calculation, PBI-COFs was simplified into **PBI-COF** nanosheets composed of four adjacent hexagonal pores. The initial model consisted of four nanosheets, 20 $LiBF_4$ molecules and 200 PC molecules, all of which were randomly distributed. The calculations of molecular dynamics simulation were performed for lithium-ion transport in PC solution and **$LiBF_4$/PC@ PBI-COF** using the Forcite module. COMPASSⅢ was used as the molecular force field. The time step is 1 fs. The systems were brought to 298K and simulated for 2 ns in total.

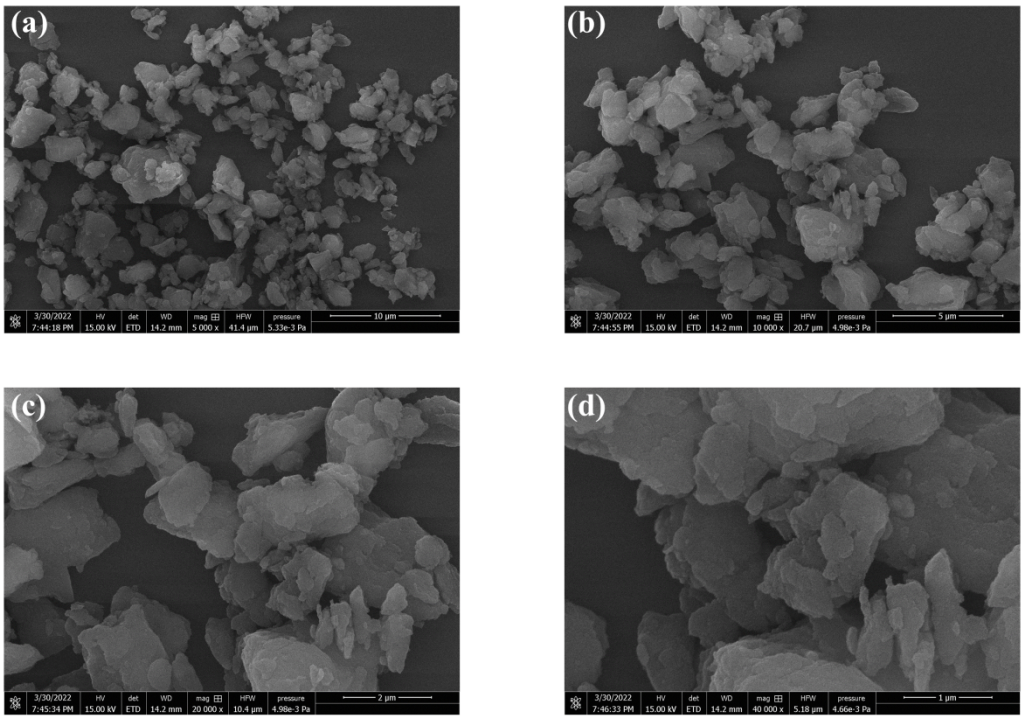

Fig. S1: SEM image of **PBI-COF** at different magnifications.

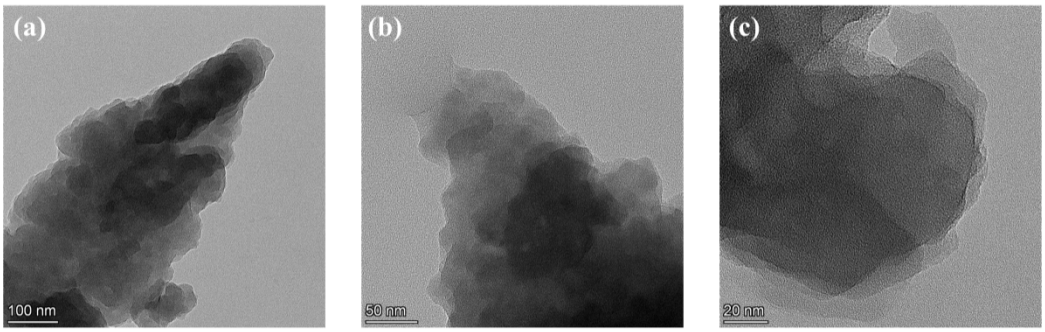

Fig. S2: HRTEM images of **PBI-COF**.

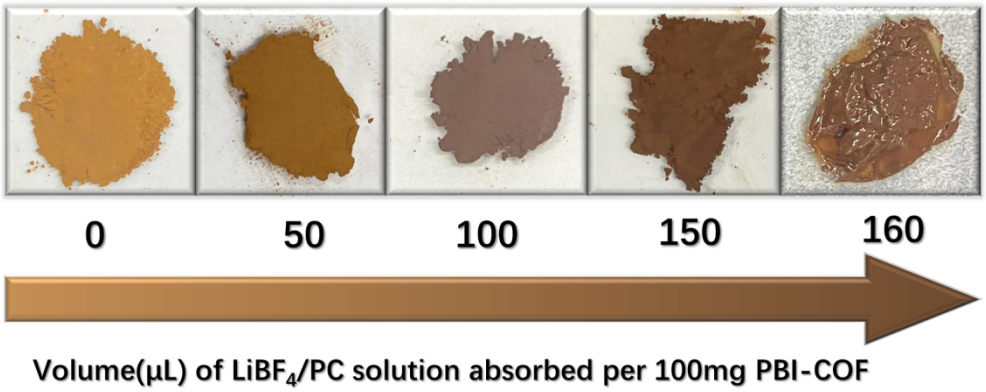

Fig. S3: Optical photograph of **LiBF$_4$/PC@PBI-COF-*X*** (*X* = 0, 50, 100, 150, 160), respectively.

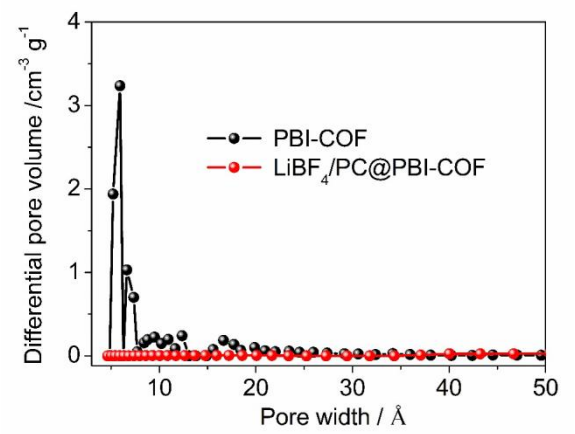

Fig. S4: Pore size distribution of **PBI-COF** (black) and **LiBF$_4$/PC@PBI-COF** (red).

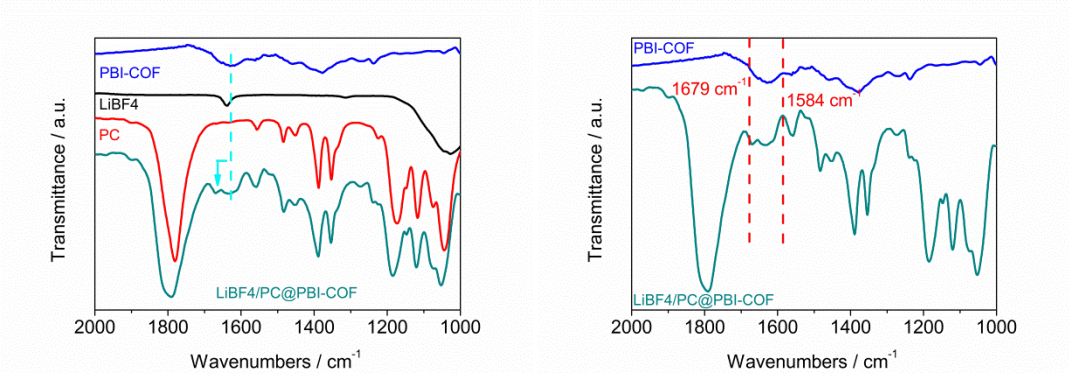

Fig. S5: FT-IR spectra of **LiBF$_4$/PC@PBI-COF** (green); **PBI-COF** (blue); PC (red) and $LiBF_4$ (black).

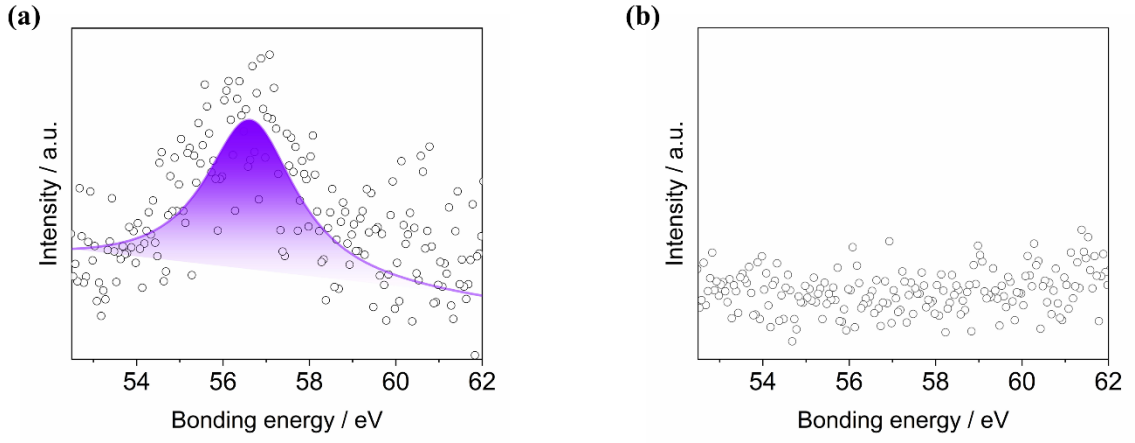

Fig. S6: High resolution Li 1s XPS spectra: (a) **$LiBF_4$/PC@PBI-COF** and (b) **PBI-COF**.

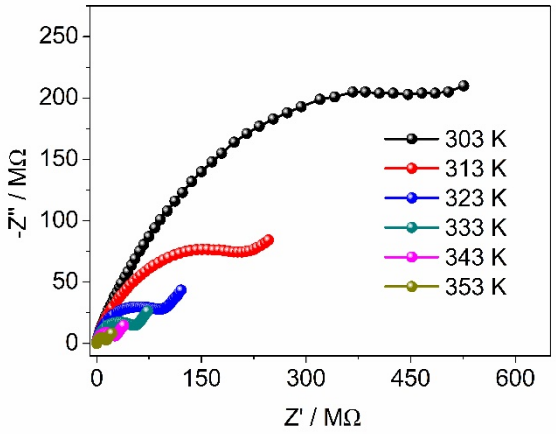

Fig. S7: Nyquist plots of **PBI-COF** at selected temperatures.

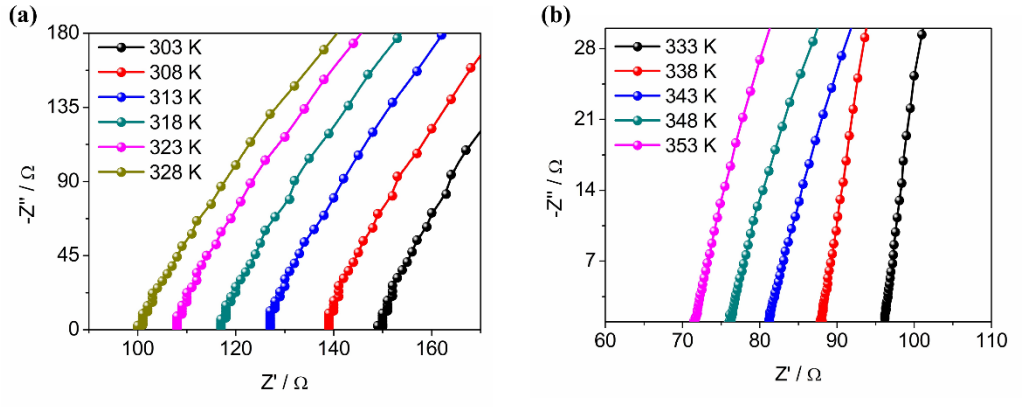

Fig. S8: Nyquist plots of **$LiBF_4$/PC@PBI-COF** at the selected temperatures of (a) 303–328 K and (b) 333–353 K.

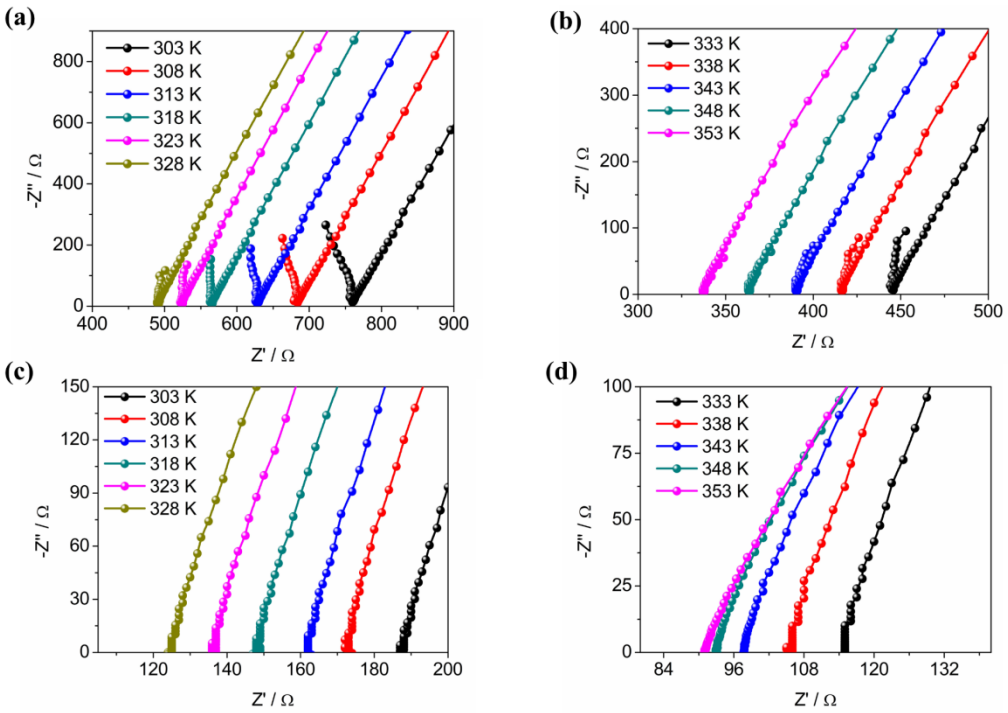

Fig. S9: Nyquist plots: (a, b) **$LiBF_4$/PC@PBI-COF-50**, (c, d) **$LiBF_4$/PC@PBI-COF-100** at the selected temperatures.

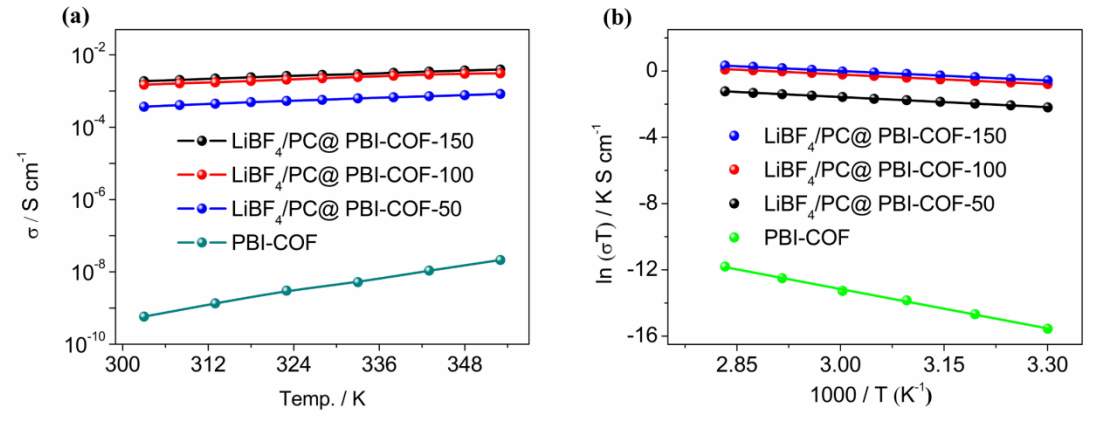

Fig. S10: (a) Temperature dependent conductivity, (b) Arrhenius plots of **PBI-COF**, **$LiBF_4$/PC@PBI-COF-50**, **$LiBF_4$/PC@PBI-COF-100**, **$LiBF_4$/PC@PBI-COF-150**.

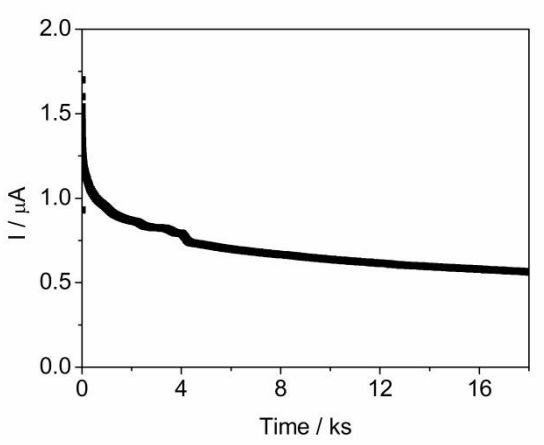

Fig. S11: Current–time curves of Li|**$LiBF_4$/PC@Celgard2400**|Li at 10 mV of polarization voltage.

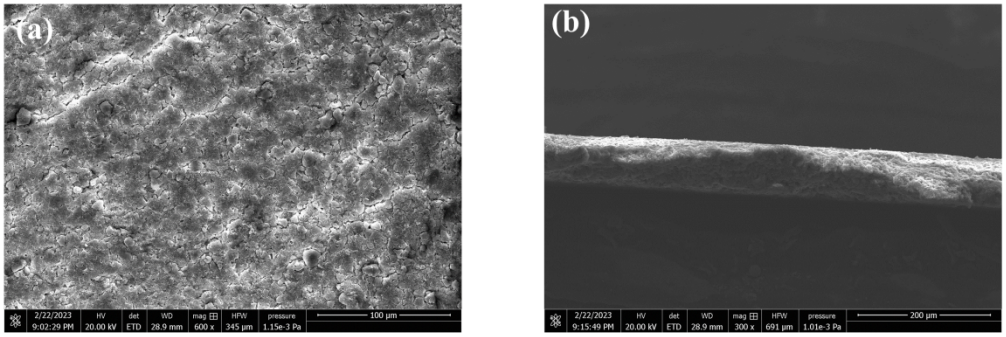

Fig. S12: SEM images: (a) surface morphology and (b) cross section of **$LiBF_4$/PC@PBI-COF/PTFE** membrane.

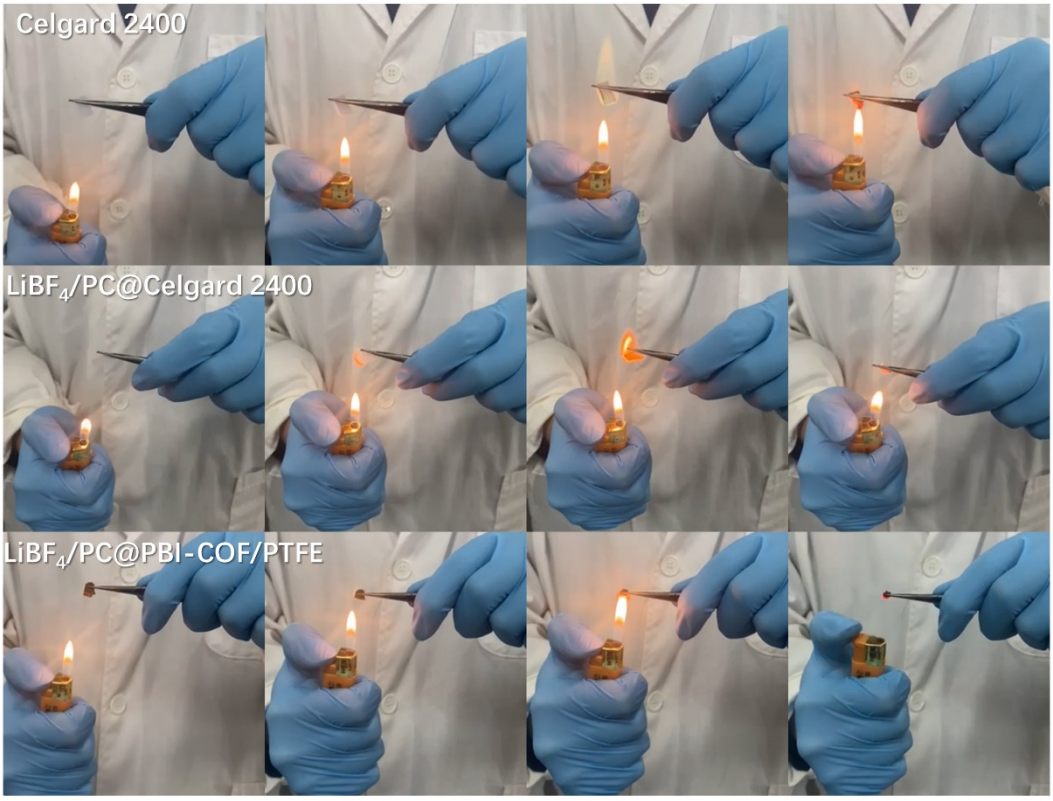

Fig. S13: Combustibility test of Celgard2400 membrane, $LiBF_4$/PC@Celgard2400 membrane and **$LiBF_4$/PC@PBI-COF/PTFE**, respectively.

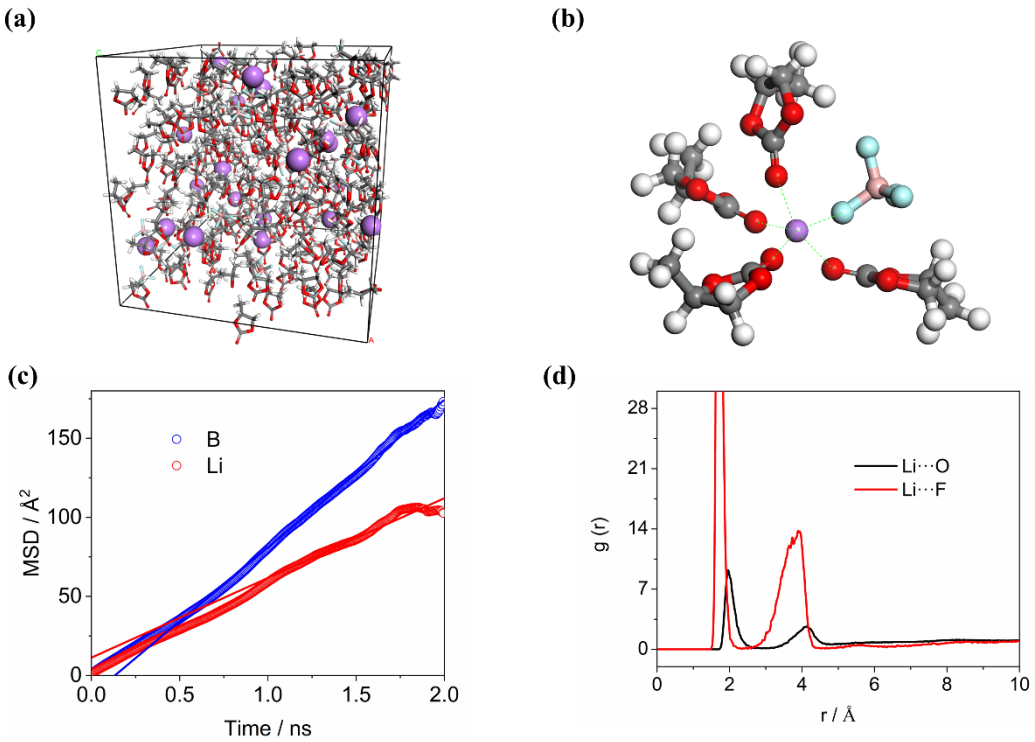

Fig. S14: (a) Illustration of the initial molecular dynamics (MD) model with $LiBF_4$/PC, (b) MD snapshot of Li^+ ion solvated shell in $LiBF_4$/PC, (c) calculated mean square displacement (MSD) of Li^+ and BF_4^- ions as a function of the simulation time, (d) radial distribution functions (RDF) of Li^+ in $LiBF_4$/PC.

Table S1: Summary of COF-based solid electrolyte properties

Materials	Ionic conductivity / S cm^{-1}	t_+	Ref.
ICOFs	3.05×10^{-5}	0.8	1
CD-COFs	2.7×10^{-3}(30°C)	/	2
Li-CON-TFSI	5.74×10^{-5} (30°C) 2.09×10^{-4} (70°C)	0.61	3
Li^+@TPB-BMTP-COF	6.04×10^{-6} (40°C) 2.85×10^{-5} (60°C) 1.66×10^{-4} (80°C) 5.49×10^{-4} (90°C)	/	4
TpPa-SO_3Li	2.70×10^{-5} (30°C)	0.90	5
CH_3-Li-ImCOF	8.00×10^{-5} (30°C)	0.93	6
PEG-Li^+@EB-COF-ClO_4	1.93×10^{-5}(30°C) 1.78×10^{-3}(120°C)	0.60	7
Ge-COF-1	4.36×10^{-6} (20°C)	0.83	8
Li-CON-3	0.90×10^{-5} (−40°C) 3.21×10^{-5} (20°C) 1.17×10^{-4} (100°C)	0.92	9
Im-COF-TFSI@Li	2.92×10^{-5} (30°C) 4.64×10^{-4} (80°C) 4.04×10^{-3} (150°C)	0.62	10
dCOF-ImTFSI-60	9.74×10^{-5}(RT) 1.03×10^{-3}(80°C) 7.05×10^{-3}(150°C)	0.72	11
Q-COF	7.50×10^{-5} (30°C) 1.50×10^{-4} (60°C)	0.72	12
TPB-DMTP-COF	1.3×10^{-4}(30°C) 1.26×10^{-3}(60°C)	0.13	13
COF-PEG-B3-Li	3.4×10^{-6}(60°C) 1.5×10^{-3}(200°C)	0.18	14
LPC-2	4.36×10^{-4}(60°C) 4.90×10^{-3}(100°C) 1.42×10^{-2}(150°C)	0.58	15
TpPa–SO_3H@PP	1.8×10^{-4} (30°C)	0.9	16
CNT@COF	1.85×10^{-3} (30°C)	0.78	17
LiO_3S-COF2	5.47×10^{-5}(30°C)	0.93	18
LiOOC-COF3	1.36×10^{-5}(30°C) 1.1×10^{-4}(80°C)	0.91	19
COF-Cl@PP	7.8×10^{-4} (30°C)	0.82	20
COF-F@PP	7.6×10^{-4} (30°C)	0.87	20

Notes and References

1. Y. Du, H. Yang, J. M. Whiteley, S. Wan, Y. Jin, S.-H. Lee and W. Zhang, Ionic Covalent Organic Frameworks with Spiroborate Linkage, *Angew. Chem. Int. Ed*., 2016, **55**, 1737 –1741.
2. Y. Zhang, J. Duan, D. Ma, P. Li, S. Li, H. Li, J. Zhou, X. Ma, X. Feng and B. Wang, Three-Dimensional Anionic Cyclodextrin-Based Covalent Organic Frameworks, *Angew. Chem. Int. Ed*., 2017, **56**, 16313 –16317.
3. H. Chen, H. Tu, C. Hu, Y. Liu, D. Dong, Y. Sun, Y. Dai, S. Wang, H. Qian, Z. Lin and L. Chen, Cationic Covalent Organic Framework Nanosheets for Fast Li-Ion Conduction, *J. Am. Chem. Soc*., 2018, **140**, 896−899.
4. Q. Xu, S. Tao, Q. Jiang and D. Jiang, Ion Conduction in Polyelectrolyte Covalent Organic Frameworks, *J. Am. Chem. Soc*., 2018, **140**, 7429−7432.
5. K. Jeong, S. Park, G. Y. Jung, S. H. Kim, Y.-H. Lee, S. K. Kwak and S.-Y. Lee, Solvent-Free, Single Lithium-Ion Conducting Covalent Organic Frameworks, *J. Am. Chem. Soc*., 2019, **141**, 5880−5885.
6. Y. Hu, N. Dunlap, S. Wan, S. Lu, S. Huang, I. Sellinger, M. Ortiz, Y. Jin, S.-H. Lee and W. Zhang, Crystalline Lithium Imidazolate Covalent Organic Frameworks with High Li-Ion Conductivity, *J. Am. Chem. Soc*., 2019, **141**, 7518−7525.
7. Z. Guo, Y. Zhang, Y. Dong, J. Li, S. Li, P. Shao, X. Feng and B. Wang, Fast Ion Transport Pathway Provided by Polyethylene Glycol Confined in Covalent Organic Frameworks, *J. Am. Chem. Soc*., 2019, **141**, 1923−1927.
8. S. Ashraf, Y. Zuo, S. Li, C. Liu, H. Wang, X. Feng, P. Li and B. Wang, Crystalline Anionic Germanate Covalent Organic Framework for High CO_2 Selectivity and Fast Li Ion Conduction, *Chem. Eur. J*., 2019, **25**, 13479 – 13483.
9. X. Li, Q. Hou, W. Huang, H.-S. Xu, X. Wang, W. Yu, R. Li, K. Zhang, L. Wang, Z. Chen, K. Xie and K. P. Loh, Solution-Processable Covalent Organic Framework Electrolytes for All-Solid-State Li-Organic Batteries, *ACS Energy Lett*., 2020, **5**, 3498−3506.

10. Z. Li, Z.-W. Liu, Z.-J. Mu, C. Cao, Z. Li, T.-X. Wang, Y. Li, X. Ding, B.-H. Han and W. Feng, Cationic Covalent Organic Framework Based All-Solid-State Electrolytes, *Mater. Chem. Front*., 2020, **4**, 1164.
11. Z. Li, Z.-W. Liu, Z. Li, T.-X. Wang, F. Zhao, X. Ding, W. Feng and B.-H. Han, Defective 2D Covalent Organic Frameworks for Postfunctionalization, *Adv. Funct. Mater*., 2020, **30**, 1909267.
12. C. Niu, W. Luo, C. Dai, C. Yu and Y. Xu, High-Voltage-Tolerant Covalent Organic Framework Electrolyte with Holistically Oriented Channels for Solid-State Lithium Metal Batteries with Nickel-Rich Cathodes, *Angew. Chem. Int. Ed*., 2021, **60**, 24915 – 24923.
13. Z. Wang, W. Zheng, W. Sun, L. Zhao and W. Yuan, Covalent Organic Frameworks-Enhanced Ionic Conductivity of Polymeric Ionic Liquid-Based Ionic Gel Electrolyte for Lithium Metal Battery, *ACS Appl. Energy Mater*., 2021, **4**, 2808−2819.
14. Y. Wang, K. Zhang, X. Jiang, Z. Liu, S. Bian, Y. Pan, Z. Shan, M. Wu, B. Xu and G. Zhang, Branched Poly(ethylene glycol)-Functionalized Covalent Organic Frameworks as Solid Electrolytes, *ACS Appl. Energy Mater*., 2021, **4**, 11720−11725.
15. Z. Wu, Q. Xu, J. Li and X.-M. Zhang, Liquid-Like Phase of *N, N*-Dimethylpyrrolidinium Iodide Impregnated into COFs Endows Fast Lithium Ion Conduction in the Solid State, *Chem. Eur. J*., 2021, **27**, 4583 – 4587.
16. J. Zhao, G. Yan, X. Zhang, Y. Feng, N. Li, J. Shi and X. Qu, In Situ Interfacial Polymerization of Lithiophilic COF@PP and POP@PP Separators with Lower Shuttle Effect and Higher Ion Transport for High-Performance Li-S Batteries, *Chem. Eng. J*., 2022, **442***,* 136352.
17. W. Yan, X. Gao, J.-L. Yang, X. Xiong, S. Xia, W. Huang, Y. Chen, L. Fu, Y. Zhu and Y. Wu, Boosting Polysulfide Catalytic Conversion and Facilitating Li^+ Transportation by Ion-Selective COFs Composite Nanowire for Li-S Batteries, *Small*, 2022, **18**, 2106679.

18. Y. Sun, G. Zhao, Y. Fu, Y. Yang, C. Zhang, Q. An and H. Guo, Understanding a Single-Li-Ion COF Conductor for Being Dendrite Free in a Li-Organic Battery, *Research*, 2022, **3**, 1-10.
19. G. Zhao, Z. Mei, L. Duan, Q. An, Y. Yang, C. Zhang, X. Tan and H. Guo, COF‐Based Single Li^+ Solid Electrolyte Accelerates the Ion Diffusion and Restrains Dendrite Growth in Quasi‐Solid‐State Organic Batteries, *Carbon Energy*, 2023, **5**, e248.
20. S. Yao, Y. Yang, Z. Liang, J. Chen, J. Ding, F. Li, J. Liu, L. Xi, M. Zhu and J. Liu, A Dual-Functional Cationic Covalent Organic Frameworks Modified Separator for High Energy Lithium Metal Batteries, *Adv. Funct. Mater*. 2023, 2212466.